Nanoscale

Accepted Manuscript

Downloaded by National University of Singapore on 23 March 2012
Published on 19 March 2012 on http://pubs.rsc.org | doi:10.1039/C2NR30557G

Nanoscale

www.rsc.org/nanoscale
Volume 2 | Number 1 | January 2010 | Pages 1–156

ISSN 2040-3364

RSC Publishing

COVER ARTICLE
Graham *et al.*
Mixed metal nanoparticle assembly and the effect on surface-enhanced Raman scattering

REVIEW
Lin *et al.*
Progress of nanocrystalline growth kinetics based on oriented attachment

2040-3364(2010)2:1;1-T

This is an *Accepted Manuscript*, which has been through the RSC Publishing peer review process and has been accepted for publication.

Accepted Manuscripts are published online shortly after acceptance, which is prior to technical editing, formatting and proof reading. This free service from RSC Publishing allows authors to make their results available to the community, in citable form, before publication of the edited article. This *Accepted Manuscript* will be replaced by the edited and formatted *Advance Article* as soon as this is available.

To cite this manuscript please use its permanent Digital Object Identifier (DOI®), which is identical for all formats of publication.

More information about *Accepted Manuscripts* can be found in the **Information for Authors**.

Please note that technical editing may introduce minor changes to the text and/or graphics contained in the manuscript submitted by the author(s) which may alter content, and that the standard **Terms & Conditions** and the **ethical guidelines** that apply to the journal are still applicable. In no event shall the RSC be held responsible for any errors or omissions in these *Accepted Manuscript* manuscripts or any consequences arising from the use of any information contained in them.

Functional Hybrid Nickel Nanostructures as Recyclable SERS Substrates: Detection of Explosives and Biowarfare Agents

P. R. Sajanlal and T. Pradeep*

DST Unit of Nanoscience (DST UNS), Department of Chemistry, Indian Institute of Technology Madras, Chennai 600 036, India

*Address correspondence to pradeep@iitm.ac.in

Fax: + 91-44 2257-0545

ABSTRACT

We present the creation of highly anisotropic nickel nanowires (NWs) and large area, free-standing carpets extending over cm^2 area by simple solution phase chemistry. The materials can be post synthetically manipulated to produce hybrid tubes, wires, and carpets by galvanic exchange reactions with Au^{3+}, Ag^{+}, Pt^{2+}, and Pd^{2+}. All of these structures, especially the hybrid carpets and tubes have been prepared in bulk and are surface enhanced Raman scattering (SERS) active substrates. Molecules of relevance such as dipicolinic acid (constituting 5-15% of the dry weight of bacterial spore of Bacillus anthracis), dinitrotoluene, hexahydro-1,3,5-triazine (RDX), and trinitrotoluene at nanomolar concentrations have been detected. An enhancement factor of ~10^{10} was observed for the Ni/Au nanocarpet. The reusability of the Ni/Au nanocarpet for SERS applications was tested 5 times without affecting the sensitivity. The reusability and sensitivity over large area has been demonstrated by Raman microscopy. Our method provides an easy and cost effective way to produce recyclable, large area, SERS active substrates with high sensitivity and reproducibility which can overcome the limitation of one-time use of traditional SERS substrates.

Keywords: functional nanomaterials, SERS, reusable substrate, galvanic replacement reaction, explosives

1. INTRODUCTION

Detection of trace amounts of explosives and chemical warfare agents is an important task in view of national security and defense. Potentially harmful materials such as disease causing bacterial spores, viruses, and toxins have to be identified at low concentrations quickly and accurately for the safety and well-being of the population. Though various detection techniques are available, systematic efforts have been ongoing to develop better analytical techniques to detect a multitude of hazardous materials in a cost-effective, rapid, and reliable manner. Anisotropic micro/nano materials with well-defined physiochemical properties are of great interest to materials chemists in view of their morphology-, size-, and crystallinity-dependent intrinsic properties as well as attractive applications in the fields of catalysis, sensing, electronics, and bio-related applications.[1-3]

Surface enhanced Raman scattering (SERS)[4-10] is a phenomenon, exhibited by certain nanoparticles (NPs) which enables the rapid detection of molecules down to single molecule level, at ambient conditions. Highly anisotropic NPs such as triangles,[11, 12] stars,[13] flowers,[4] etc. [4-9, 11, 14] are well-known for their excellent SERS activity and related applications.[15] Nanoparticles assemblies such as superlattices[16] also show similar enhancement, enabling them for sensing applications.[17] Theoretical predictions of field enhancement around various anisotropic nanostructures have been reported.[13, 18, 19] However, cost-effective production of a robust, reusable, large-area, and homogeneous SERS substrate with high sensitivity and reproducibility still remains an important issue. In view of making appropriate and affordable SERS substrates, synthesizing SERS active nanomaterials by making thin coating of Au or Ag on prefabricated, cheap substrates gained popularity.[20, 21] Periodic array of SERS active nanostructures can also be fabricated in large area by nanosphere lithography techniques.[22] Most of these techniques have the major disadvantage of being very time consuming with high production costs. Solution based synthesis of most of the anisotropic nanomaterials requires various surfactants such as cetyltrimethylammonium bromide (CTAB) and sodium dodecyl sulfate (SDS) and polymers such as poly(N-vinyl-2-pyrrolidone) (PVP) and polyamines. The presence of such organic coating may reduce the efficiency and sensitivity of these NPs towards SERS activity.

The galvanic displacement reaction[23-28] is an easy way to make SERS active nanomaterials from a pre-fabricated NPs template. The galvanic displacement reaction has advantages over the other methods in synthesizing nanostructures since no surfactant or coordinating molecules are involved in the synthesis which can yield clean surfaces, and is an important attribute for surface enhanced spectroscopies. Here, we report the synthesis of thorny nickel nanowires (NWs) and nanocarpets (NC) via a simple chemical reduction route and their subsequent use as sacrificial templates for making highly SERS active, hybrid anisotropic materials such as Au/Ni NCs, NWs and nanotubes through galvanic displacement reaction. Nickel NPs are very good candidates to use as sacrificial template for making SERS active noble metal nanomaterials, as Ni is relatively cheap and having lower reduction potential (0.25 V for Ni^{2+}/Ni (*vs* standard hydrogen electrode (SHE))) than noble metal ions (0.99 V for $AuCl_4^-/Au$, 0.76 V for $PtCl_4^{2-}/Pt$, and 0.59 V for $PdCl_4^{2-}/Pd$)). Such hybrid materials show enhanced oxidation-resistance and stability, which make them useful for certain biological applications, catalysis and SERS.[29-31] Various other nanosystems like Ni/Pd nanotubes, Ni/Pt and Ni/Ag NWs were also made to demonstrate the viability of our method to make various hybrid nanomaterials. Reusability and utility of the Ni/Au NCs in the detection of biomolecules, explosives, and an explosive surrogate at very low concentrations has been demonstrated using Raman spectroscopy and microscopy. Creation of such inexpensive, free standing, recyclable, large area SERS substrates by a fast chemistry without the aid of templates or surfactants is advantageous for developing applications.

2. EXPERIMENTAL

2.1. Materials

$NiCl_2 \cdot 6H_2O$, $HAuCl_4.2H_2O$, $PdCl_2$, and hydrazine monohydrate were purchased from SD Fine Chemicals, India (AR grade). Hexachloroplatinic acid ($H_2PtCl_6 \cdot 6H_2O$) dipicolinic acid (DPA), and 2,4-dinitrotoluene (DNT) were purchased from Sigma Aldrich. Trinitrotoluene (TNT) and hexahydro-1,3,5-triazine (RDX) were gifts from Indira Gandhi Centre for Atomic Research, Kalpakkam, India. All chemicals were used as such without further purification. Triply distilled water was used throughout the experiments.

2.2. Synthesis of nickel nanowires and nanocarpets

Ni NWs were synthesized by the reduction of nickel chloride in water using concentrated aqueous hydrazine hydrate (HyH) solution as the reducing agent. In a typical synthesis, 1 mL of 250 mM aqueous solution of nickel chloride was added to 9 mL of water at 80 ^oC to get 25 mM solution of Ni^{2+}. After about one minute, 1 mL of HyH solution was added drop-wise into the solution. No stirring was done during this process. After the addition of HyH, NCs were formed gradually inside the wall of the glass beaker as a silverish film after 5 min. These NCs measuring an area of ~5 cm^2 were then peeled carefully off the beaker. Ni NWs were formed simultaneously inside the solution as black network-like residue, which was separated by forceps. The NCs and NWs were washed carefully with distilled water and subsequently with alcohol, to remove excess of hydrazine and the other unreacted ions. The methodology could be scaled to get larger quantities of these materials of the order of grams.

2.3. Making of hybrid Ni nanotubes and wires

About 4 mg of the Ni NWs, synthesized as per the above procedure, were immersed inside 500 μL of 10 mM $HAuCl_4$ or H_2PdCl_4 solution in a vial. This solution was shaken gently for 5 min. After that, as formed Ni/Au and Ni/Pd nanotubes were separated out from the solution using a bar magnet. They were then washed carefully with distilled water and subsequently with alcohol, to remove unreacted ions.

In order to make hybrid Ni/Ag and Ni/Pt NWs the aforementioned experiment was conducted using 500 µL of 25 mM H_2PtCl_6 or $AgNO_3$ in place of Au and Pd precursors.

2.4. Ni/Au nanocarpets

Thin films of nickel NCs (4 mg, ~2 cm^2) were immersed inside 500 µL of 10 mM of $HAuCl_4$ in a vial for about 5 min. A visible change from silverish to light brown color indicates the formation of Ni/Au NCs. The Ni/Au NCs were separated out carefully from the solution using forceps, washed with distilled water and subsequently with alcohol and dried. This material was later used for SERS measurements.

In all the above mentioned cases of synthesis of hybrid nanostructures, varying quantities of metal ions were added to the Ni nanostructures to deposit the required amount of metals on them.

3. INSTRUMENTATION

Scanning electron microscopy (SEM) imaging and energy dispersive analysis of X-ray (EDAX) studies were done with a FEI QUANTA-200 scanning electron microscope. Raman measurements were done with a WiTec GmbH, Alpha-SNOM CRM 300 instrument having a 633 nm laser with a maximum power of 40 mW. During the Raman measurements, the laser power has been adjusted so as to get good Raman spectrum. The material was carefully transferred onto a cover glass, and required amounts of analyte solution of finite concentrations were mixed with these nanomaterials. It was then mounted onto the sample stage of the Raman spectrometer. For the SERS measurements, the backscattered light was collected using a 60x liquid immersion objective at an integration time of 1s. For Raman imaging of Ni/Au nanotubes and Ni/Au NC, the backscattered light was collected using 100x and 20x objectives, respectively, at an integration time of 50 ms. A super notch filter placed in the path of the signal effectively cuts off the excitation radiation. The signal was then dispersed using a 600 grooves/mm grating, and the dispersed light was collected by a Peltier cooled charge coupled device (CCD). Raman enhancement factors were calculated as discussed in earlier reports.[32] XPS measurements were done with Omicron ESCA Probe spectrometer with unmonochromatized Al Kα X-rays (hν = 1486.6 eV).

4. RESULTS AND DISCUSSION

Highly thorny NWs and NCs of Ni were synthesized by following the procedure mentioned in the experimental section and their morphology was studied using SEM. The NCs were separated as thin films which were several centimeters in length and width (Figure 1). The surface of the NCs attached onto the wall of the glass beaker appeared silverfish and was relatively smooth in appearance (photograph is given later, in Figure 6). The other side of the NC which was not attached to the glass wall (in contact with the solution) was highly thorny in nature and appeared as black (photograph in Figure 6). The thorns, which were projecting outward from the surface (inset of Figure 1A), gave carpet-like appearance to these films. SEM analysis revealed that these NCs were formed by the self-assembly of several flower-shaped Ni NPs of around 1µm size, as shown in Figure 1B.

Since the constituent nanoflowers were not packed densely, the NC appeared highly porous in nature (Figure 1A). The chemical composition of the Ni NCs was characterized using EDAX (Figure 1C and D). They are mainly composed of Ni along with some amount of oxygen, probably formed due to the surface oxidation of Ni (Electronic supplementary information, Fig. S1†). While carpets were formed as films, Ni NWs with 2 µm in diameter and length up to several hundred microns (Figure 1E and F) were formed in the solution as a black mass within 10 min. These were separated from the solution using forceps. Closer examination revealed that these wires were highly anisotropic, constructed by a large number of thorns with a length of 100–300 nm (Figure 1F). The NWs were highly stable. Even long time (30 min) ultrasonication could not break them, indicating that the thorn-like building blocks had fused together.

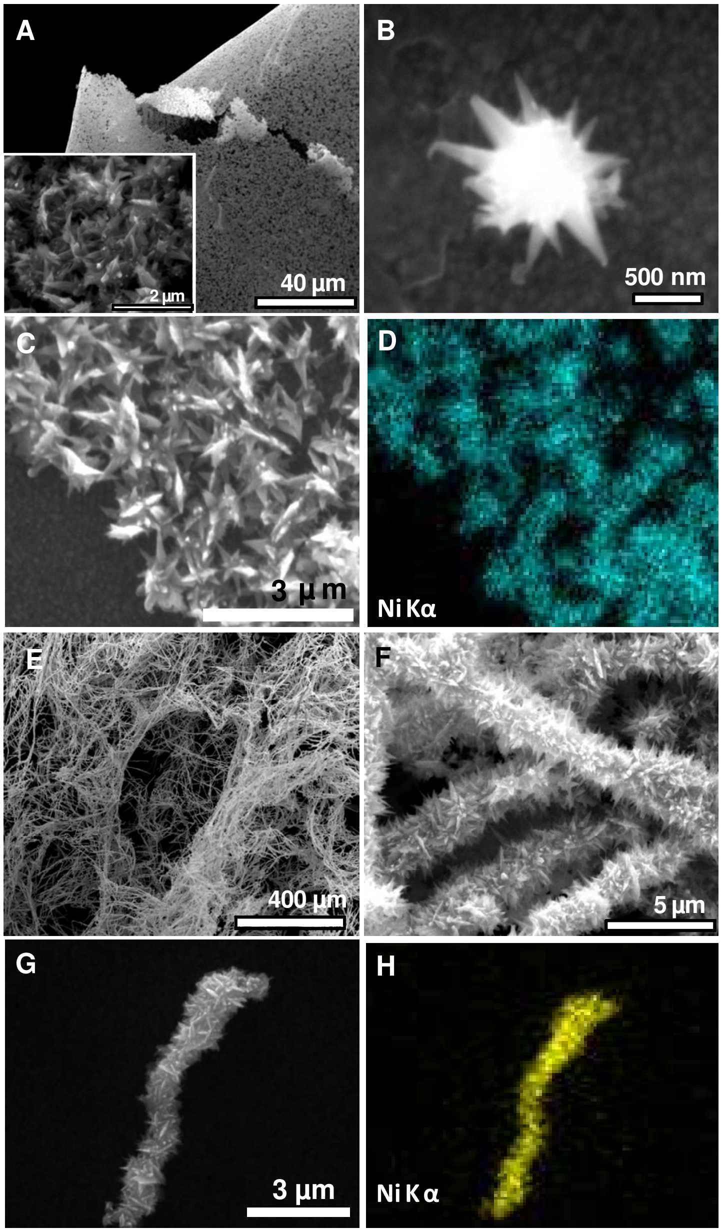

Figure 1. SEM image of Ni NC (A) and a single nanoflower (B). Inset of A is an enlarged view of the Ni NC showing the presence of thorny projections. C and D are the SEM and corresponding Ni Kα-based EDAX images of Ni NC. E and F are the SEM images of thorny Ni NWs taken at various magnifications. G and H are the SEM and corresponding EDAX images of Ni NW.

The chemical composition of the NW was examined using EDAX (Figure 1G and H). In addition to nickel, small amounts of oxygen were also present which might be attributed to the surface oxidation of nickel due to the high reactivity of elemental nickel (Electronic supplementary information, Fig. S2†).

Temperature dependence of the surface structure of these NWs has been studied. We found that the surface of the thorny NWs (Figure 2A) become fairly smooth when the reaction was carried out at elevated temperature in ethylene glycol as solvent. The synthesis yielded Ni NWs with average diameter of ~200 nm in very large quantity without any other NPs of different morphology (Figure 2A-B). The amount of HyH also plays an important role in determining the surface structure of the NW. At low concentration of HyH (100 μL), sphere-like NPs were formed and NWs were not seen (Figure 2C). Some of these particles tend to self-assemble to form chain-like structures. As the amount of HyH increases (500 μL), an increase in the number of thorns present on the NW surface was observed (Figure 2D). Further increase of the reducing agent (1 mL) resulted in the formation of highly thorny Ni NWs (Figure 2E). The number of thorns was found to decrease when excess amount of reducing agent (5 mL) was added (Figure 2F). At elevated temperature and at high concentration of the reducing agent, reduction of metal ions may happen at a faster rate, resulting in the formation of a smooth surface. Though thorny NPs and NWs of Ni were seen earlier with the assistance of surfactant and external magnetic field,[33-38] our synthetic protocol is very simple, which does not require any surfactant or magnetic field. It is proposed that at the initial stage of the reaction, $NiCl_2$ undergoes complexation with HyH. In the subsequent step, this complex is reduced by excess HyH to form smaller Ni nuclei. These nanocrystals could serve as seeds as well as provide catalytic surfaces for further growth of larger particles. Further reduction of Ni ions happens at these seed surfaces in all directions to form spherical NPs.

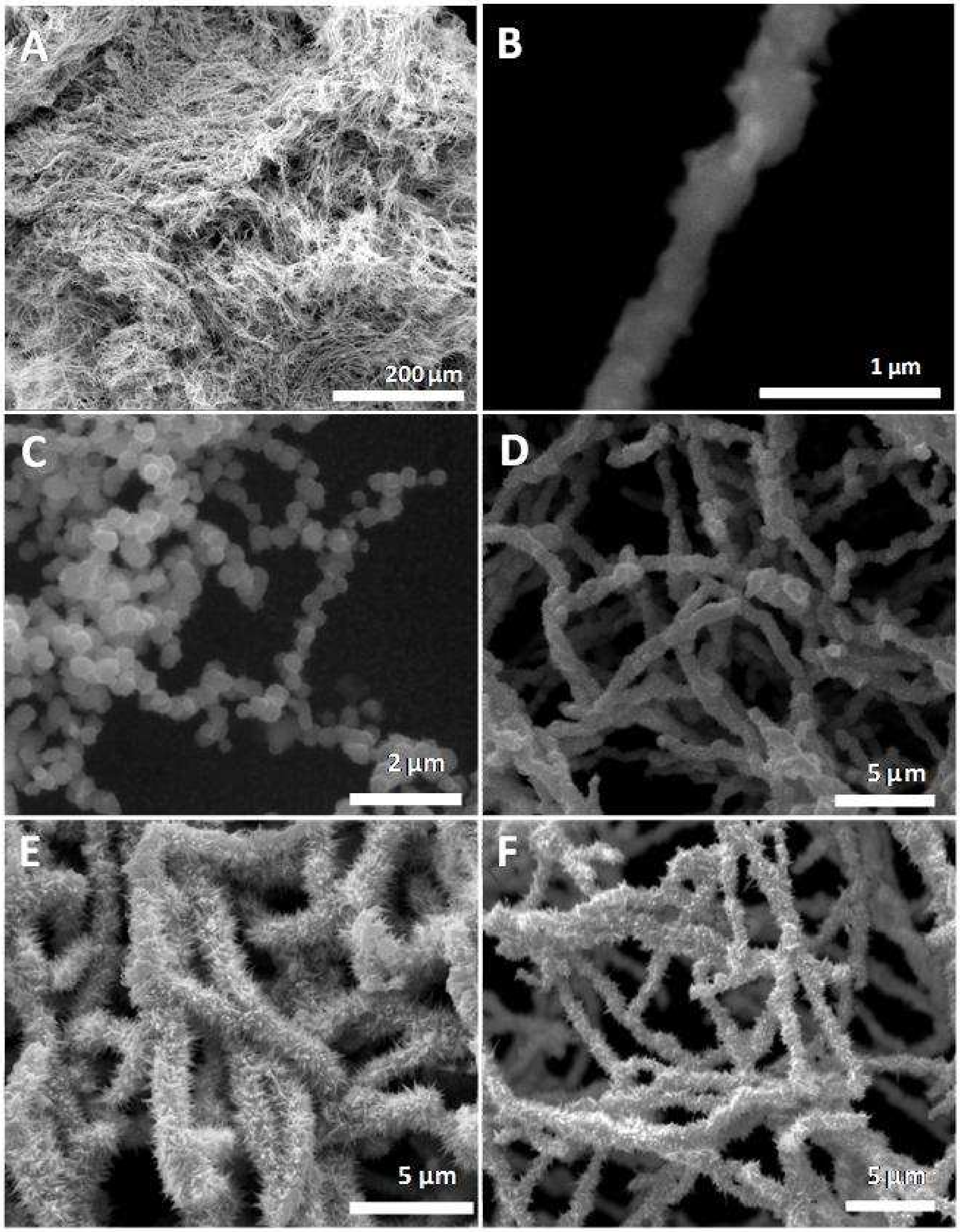

Figure 2. Large area (A) and enlarged (B) SEM images of the Ni NWs formed when ethylene glycol was used as solvent at 130 ^{0}C. C-F are the SEM images of the nanostructures synthesized using various amounts of HyH such as 0.1, 0.5, 1.0, and 5.0 mL, respectively, keeping other parameters the same.

Since the circumferential edges are having higher free energies,[39] further reduction may preferentially occur at these relatively more active sites which lead to the formation of a spiky surface. The high reducing capacity of HyH at higher temperature[40] enhances the reduction rate of Ni ions. At elevated temperature, these spiky nanospheres may tend to join each other to reduce surface energy. Subsequently, these nickel crystals would connect to form hierarchical nickel NWs. Reduction in the surface energy by the elimination of the interface during this process may facilitate NW formation. In the following steps, further deposition of Ni ions continues at these spear-like nickel stems, which grow longer toward different directions until all of the nickel ions are consumed. Continuous heating of the reaction mixture for about 30 min resulted in the formation of branched NWs (Electronic supplementary information, Fig. S3†). In the case of NC formation, the assembly of smaller nanoflowers may happen laterally in all directions which results in sheet-like structures.

4. 1. Galvanic replacement reaction

Since nickel is having a relatively lower reduction potential than noble metals, the Ni NCs and NWs have been used as sacrificial template for galvanic displacement reaction[23-26] to make hybrid systems with Au, Ag, Pt, and Pd. In such experiments, the metal nanocrystal will get oxidized by the noble metal ion which has a more positive reduction potential. In the case of Ni NWs, after the addition of Au^{3+}, interestingly we found that the NWs are getting converted to nanotubes. The resultant Ni/Au nanotubes were characterized using SEM (Figure 3). Almost all the NWs underwent galvanic displacement reaction and converted to nanotubes (Figure 3A). Figure 3B reveals the tubular nature of these hybrid nanomaterials. From the SEM images, it is clear that the tip of the NWs undergo reaction easily resulting in nanotubes with holes, mostly at the center of the tip which could be attributed to the high reactivity of the tip of such one dimensional NWs.[41] After the addition of Au^{3+} into the Ni NWs, displacement reaction happens at sites of relatively high surface energies such as point defects, stacking fault, steps, etc.[42] During the reaction, Ni atoms diffused to the surface of the NCs and Au atoms diffused into the structure. More Ni atoms on the NW surface will get displaced by Au atoms as etching creates Ni surfaces with higher surface energies. At the same time, epitaxial growth of Au results in the formation of thin film at the surface of Ni

NWs and subsequent etching will happen at the interior of the NWs, newly formed high energy Ni surfaces are now abundant. This could lead to the formation of nanotubes. Kirkendall-effect[43] is also expected to play a significant role in the formation of such nanotubes.

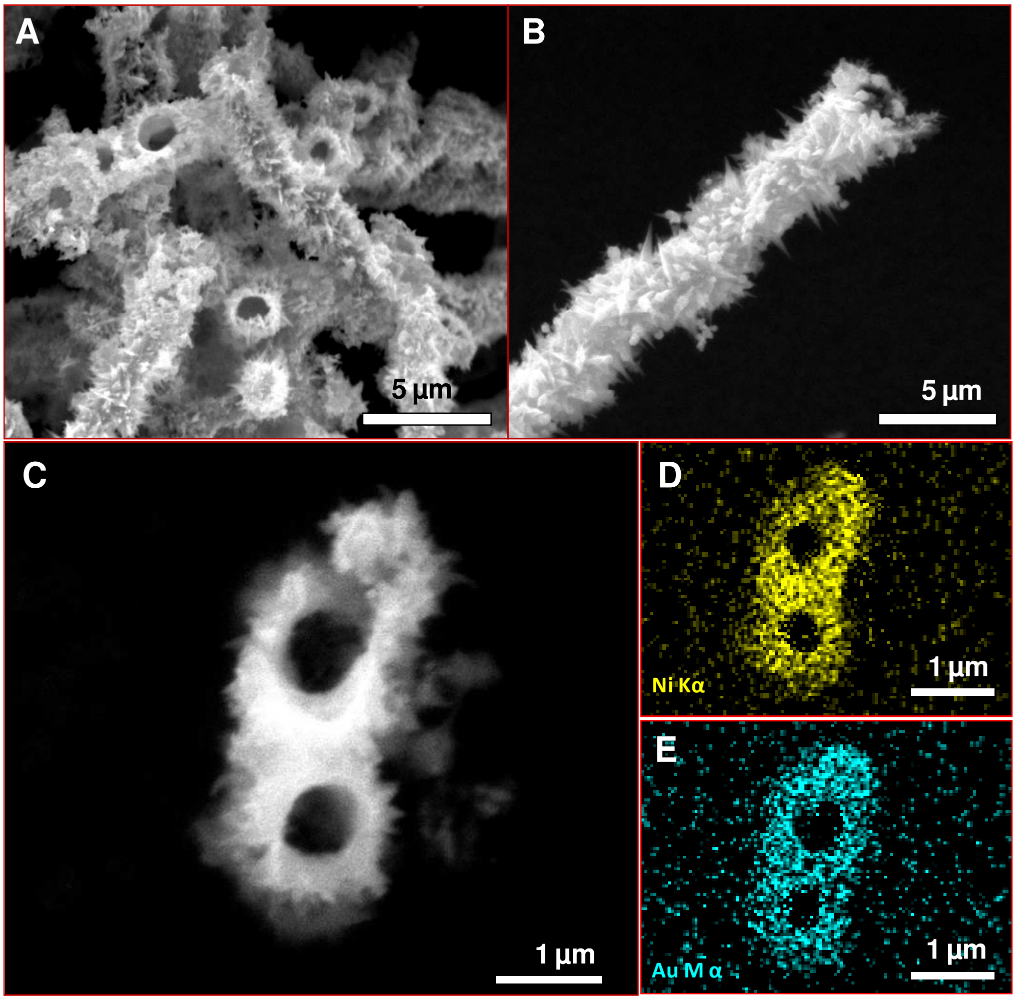

Figure 3. SEM images (A-C) of the sample $\mathbf{A_1}$ taken in various magnifications. D and E are Ni Kα and Au Mα based EDAX maps of the tip of a nanotube shown in C.

The chemical composition of these hybrid nanotubes was further confirmed by EDAX (Figure 3C-E), which shows the presence of Ni and Au. Well-defined nanotubes as shown in Figure 3 were obtained in 5 min when 500 µL of 10 mM of Au^{3+} was added into 4 mg of the Ni NWs (we refer to this sample as $\mathbf{A_1}$). Upon increasing the concentration of Au^{3+} from 10 mM to 25 mM (referred to as **A$_2$**), more amount of gold was deposited onto the Ni NWs after 5 min and the NW surface was decorated with nearly spherical gold nanobeads.

SEM images and corresponding EDAX data showing the variation in the elemental compositions of the Ni/Au nanotubes with increasing concentration of Au^{3+} are given in Figure 4. Ni/Au nanotubes formed after 5 min of addition of 500 μL of 10, 15, and 25 mM of Au^{3+} into 4 mg of Ni NWs are shown in electronic supplementary information (Fig. S4†). As reaction proceeds, more amount of Au got deposited onto the NW surface.

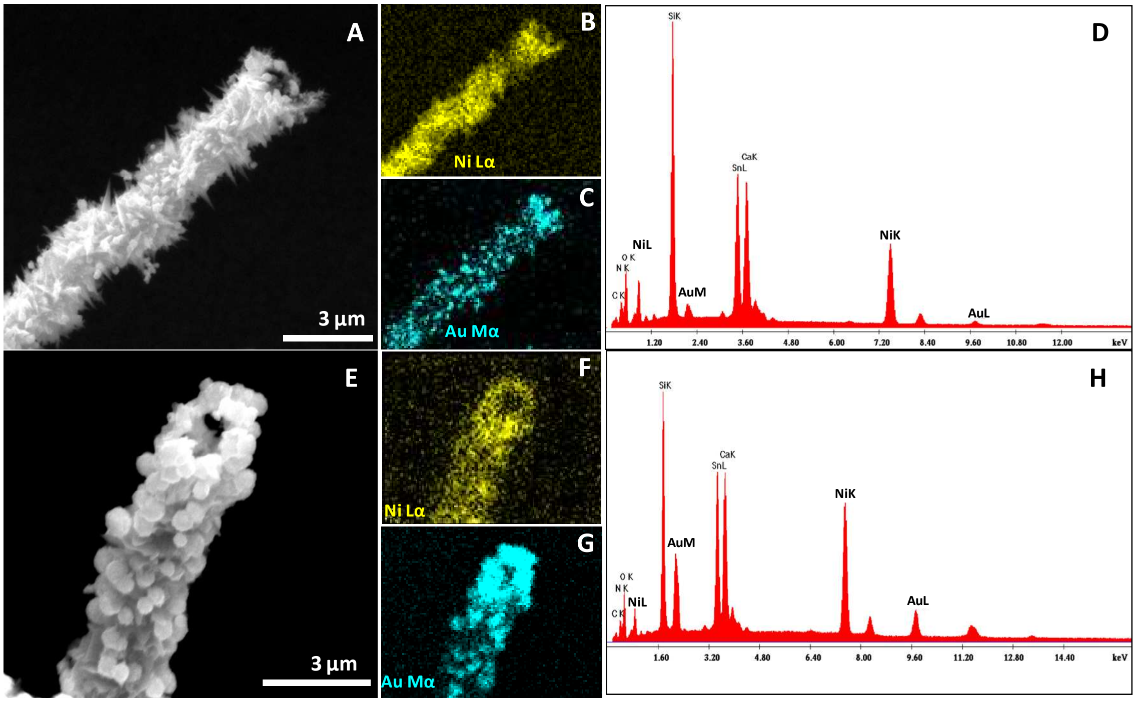

Figure 4. A and E are the SEM images of the sample **A1** and **A2**, respectively. Corresponding EDAX images and spectra are also given. The elements In, Sn and Si are due to the ITO conducting glass substrate used.

Similar approach was followed to make various hybrid nanomaterials such as Ni/Pd nanotubes, Ni/Pt, and Ni/Ag NWs. For Pd, by the addition of 500 μL of 25 mM Pd^{2+} solution, the Ni NWs were converted to Ni/Pd nanotubes as in the case of Ni/Au nanotubes (Figure 5A and B) whereas the nanotube formation was not observed for the same amount of Ag or Pt ions. At this particular concentration of metal ions, instead of forming nanotubes,

View Online

Ag and Pt got deposited onto the Ni NW surface to form hybrid Ni/Ag and Ni/Pt NWs, respectively. The large area and corresponding single particle SEM images of Ni/Pd nanotubes as well as Ni/Pt, and Ni/Ag NWs are given in Figure 5. The chemical composition of these hybrid nanostructures was characterized using EDAX (Figure 5C, D, G, H, K, and L).

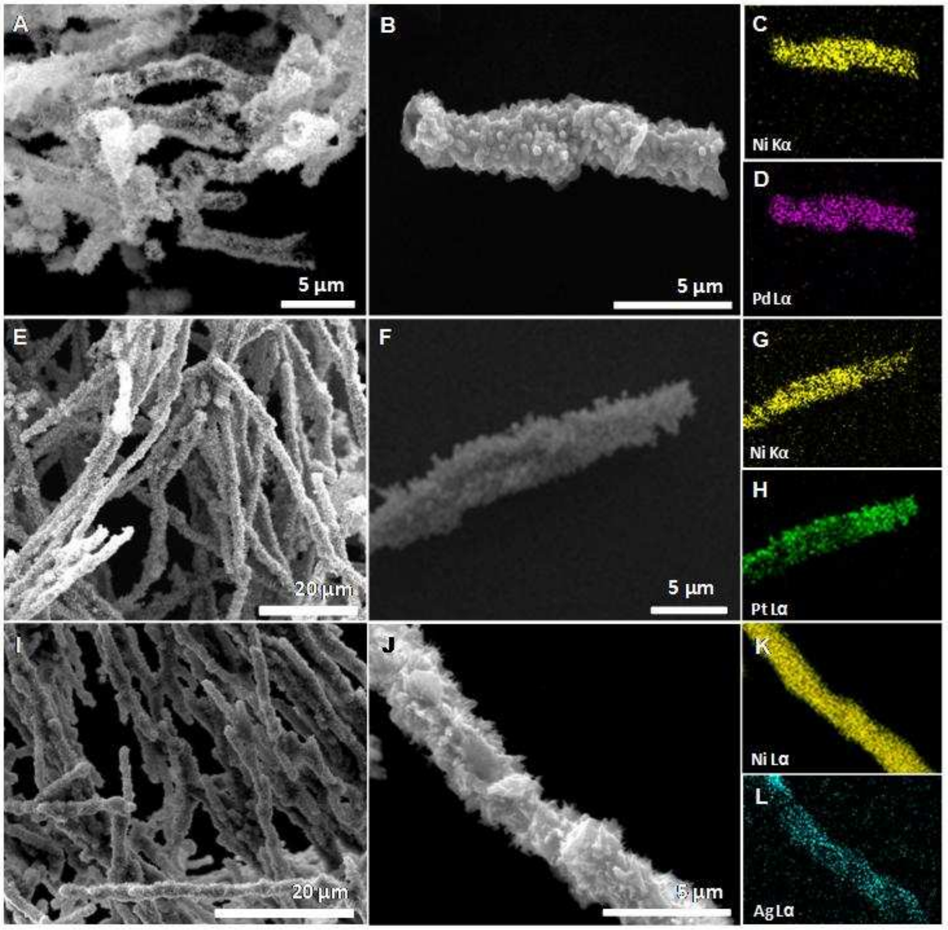

Figure 5. A, E, and I are large area SEM images Ni/Pd nanotubes, Ni/Pt, and Ni/Ag NWs, respectively. Single particle SEM images (B, F, and J) and corresponding EDAX images (C, D, G, H, K, and L) of these nanostructures are also given.

We also made bimetallic Ni/Au NCs via galvanic displacement reaction by the addition of Au^{3+} into the Ni NCs. By the addition of 500 µL of 10 mM of Au^{3+} into 4 mg of Ni NCs, we could make ~4 mg of Ni/Au bimetallic NCs (this sample is referred to as $\mathbf{B_1}$ with 2 cm^2 surface area, having almost the same morphology as the parent Ni NCs (Figure 6E). After the deposition of Au, the sharpness of the thorns reduced slightly compared to that of

Ni NCs (Figure 6D). Inset of Figure 6E shows magnified SEM image of the bimetallic NCs in which the thorns are projecting outward from the surface. Photographs of a large-area Ni NC before and after treatment with Au^{3+} solution is shown in Figure 6A-C.

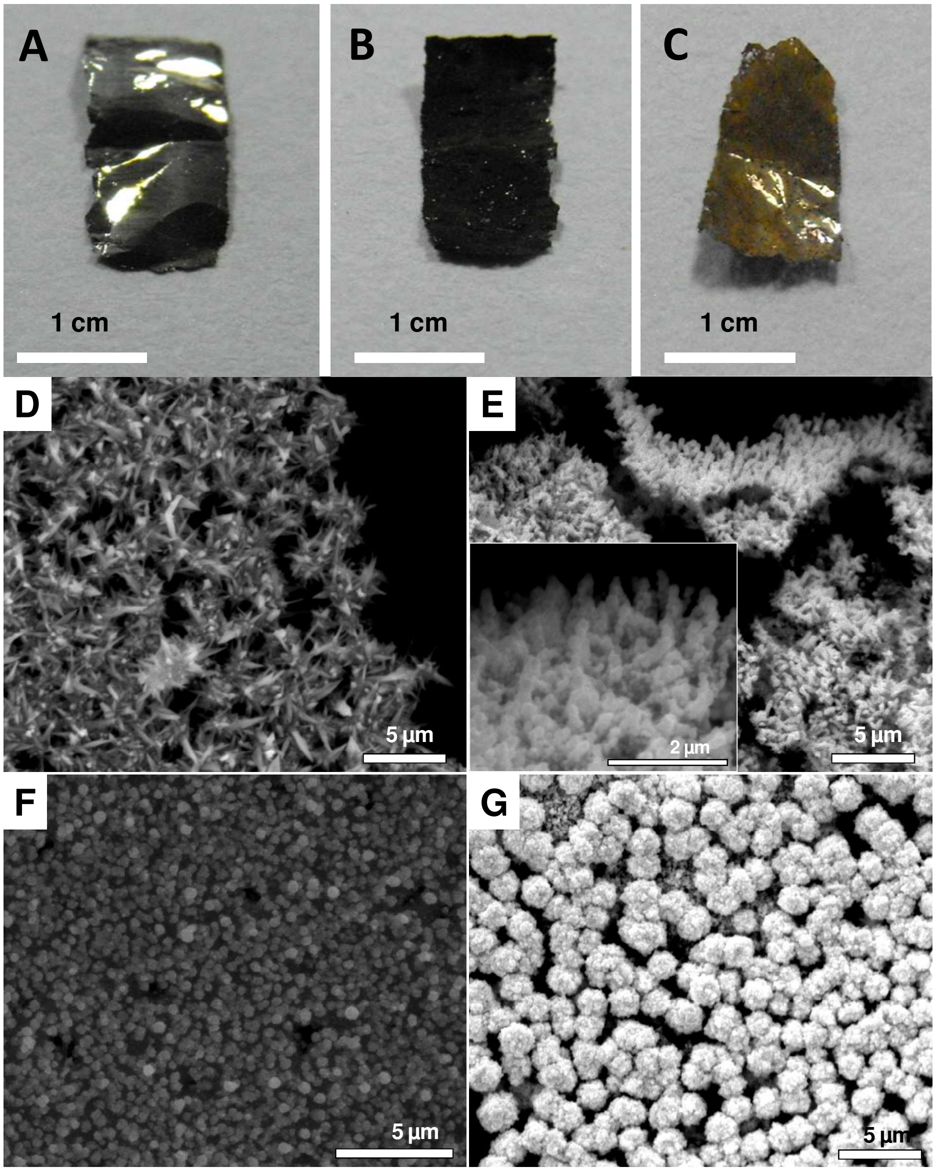

Figure 6. Photographs of the Ni NC before (A (the side attached to the glass beaker is facing the viewer) and B (the side in contact with the solution)) and after (C) treatment with Au^{3+} solution. (D) SEM image of Ni NC showing large number of spiky projections before the galvanic displacement reaction. E-G are Ni/Au NCs formed by the addition of 500 µL of 10, 15, and 25 mM of Au^{3+}, respectively, into 4 mg of Ni NCs.

As all the Au^{3+} added were not reacted with Ni atoms in the replacement reaction, a significant amount of Ni remained inside the nanocarpet (see Electronic supplementary information 5). As the reactivity at the tip of each thorn is high, displacement reaction happened to a greater extent at the tip and more amount of Au was deposited at the tip. EDAX data suggested that the ratio of atomic percentage of Au and Ni in **B1** is ~1:4 (Electronic supplementary information, Fig. S5†). More amount of Au was deposited by increasing the concentration Au^{3+} from 10 mM to 15 mM. The nanothorns present on the NCs were converted to spherical NPs with roughened surface of around 500 nm diameter, and the carpet was looking like a film made by the assembly of spheres as shown in Figure 6F. Again when the concentration of Au increased to 25 mM (referred to as $\mathbf{B_2}$), more amount of Au^{3+} got deposited and the size of the spheres increased from ~500 nm to ~ 3 μm (Figure 6G). Even after the galvanic displacement reaction, these NCs were not completely fragmented or disassembled, but existed as a film.

The chemical composition of NCs and NWs of Ni and hybrid Ni/Au NCs and nanotubes were characterized by using X-ray photoelectron spectroscopy (XPS). The wide scan XPS spectra of NCs and NWs of Ni and bimetallic Ni/Au NCs and nanotubes are given in Figure 7A. The enlarged scan of Ni 2p of Ni NCs and NWs showed $2p_{3/2}$ at ~855.5 eV and $2p_{1/2}$ at ~873.5 eV (Figure 7B). At the same time, Ni 2p region of Ni/Au NCs showed $2p_{3/2}$ at ~855.3 eV and $2p_{1/2}$ at ~873.3 eV (Figure 7C). In the case of Ni/Au nanotubes, Ni $2p_{3/2}$ and $2p_{1/2}$ were observed at ~855.4 eV and at ~873.1 eV, respectively. The observed shift in the Ni 2P peaks in all the above mentioned cases toward the higher binding energy region compared to Ni (0)(852.6 eV) can be due to the possible existence of Ni^{2+} in the form of oxide coating on the surface of these Ni nanosurfaces. The presence of satellite peaks found at high-binding energy region confirms the existence of Ni in its divalent state.[44-46] Poor intensity of the satellite features indicates that the extent of surface oxidation at the surface of Ni nanostructures is small. The O 1s peaks found around 531.4 eV in all the cases (see Electronic supplementary information, Fig. S6†) again confirms the presence of O^{2-}. The 4f region of Au in Ni/Au NCs and nanotubes are given in Figure 7D. The spectra showed the presence of Au $4f_{7/2}$ and Au $4f_{5/2}$ peaks at ~84.1 and ~87.8 eV, respectively, confirming the existence of gold in its metallic form, due to galvanic exchange.

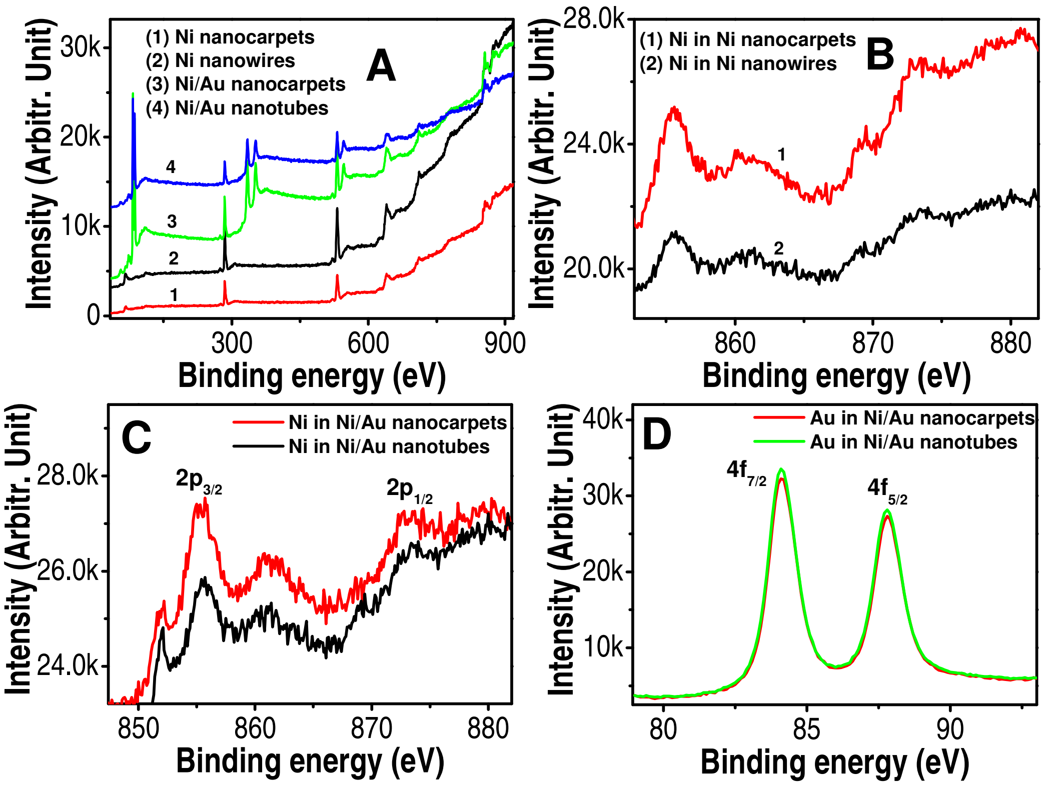

Figure 7. (A) Wide scan XPS spectra of NCs and NWs of Ni and bimetallic Ni/Au NCs and nanotubes. (B) The Ni 2p region of Ni NCs and NWs. (C) The Ni 2p region of Ni/Au NCs and nanotubes. (D) The Au 4f region of Ni/Au NCs and nanotubes.

4. 2. SERS measurements

Noble metal NPs with sharp edges and corners exhibit enhanced electric field around these locations capable of enhancing the intensity of Raman signals of molecules present there.[4, 8, 9, 47, 48] In our case, these spiky Ni/Au bimetallic nanotubes and NCs with highly roughed surfaces, devoid of any surfactants or organic species, exhibited very good SERS activity. The SERS activity of the nanomaterials has been studied using crystal violet (CV) as the analyte. For the SERS study, we selected four different substrates such as Ni/Au nanotubes (**A_1** and **A_2**) and Ni/Au NCs (**B_1** and **B_2**).

Samples **A1** and **B1** corresponding to reaction with 10 mM of Au^{3+} showed much better SERS activity compared to the other two using a higher concentration of Au^{3+}. The SERS spectra collected from various nanomaterials and corresponding SEM images are given in Figure 8. From a detailed study, we found that the sample B_1 can detect CV up to a concentration of 10^{-11} M (Electronic supplementary information, Fig. S7†) with an enhancement factor[49, 50] of the order of $\sim 10^{10}$. Even at a concentration of 10^{-11} M, we got characteristic Raman features of CV adsorbed on Ni/Au NC. The high SERS activity of Ni/Au NCs and nanotubes can be attributed to the presence of the spiky tips as well as highly corrugated surfaces acting as hot spots. Comparatively less SERS activity of the other two systems (**A2** and **B2**) can be due to the absence of the sharp thorns (due to the deposition of more amount of Au^{3+}, spiky thorns were converted into nearly spherical particles). However, they also showed SERS activity with an EF of the order of $\sim 10^7$, attributed to the presence of highly roughed surface. Apart from this, the junction between the adjacent nanospheres in the self-assembled film or wires can also act as hot spots, capable of enhancing the intensity of Raman signals. Recently, Mirkin *et al.* have showed that very long range SERS is possible in a nickel NW separated by a pair of gold nanodisks by the excitation of the surface-plasmon resonance from the gold nanodisk pair.[51] A Raman image of a Ni/Au nanotube created by integrating the spectral intensities of adsorbed CV molecules (10^{-8} M) between the 1200-1700 cm^{-1} window is shown in Figure 8B. From the Raman image, it is clear that the enhancement of the Raman features is not uniform throughout the nanotubes.

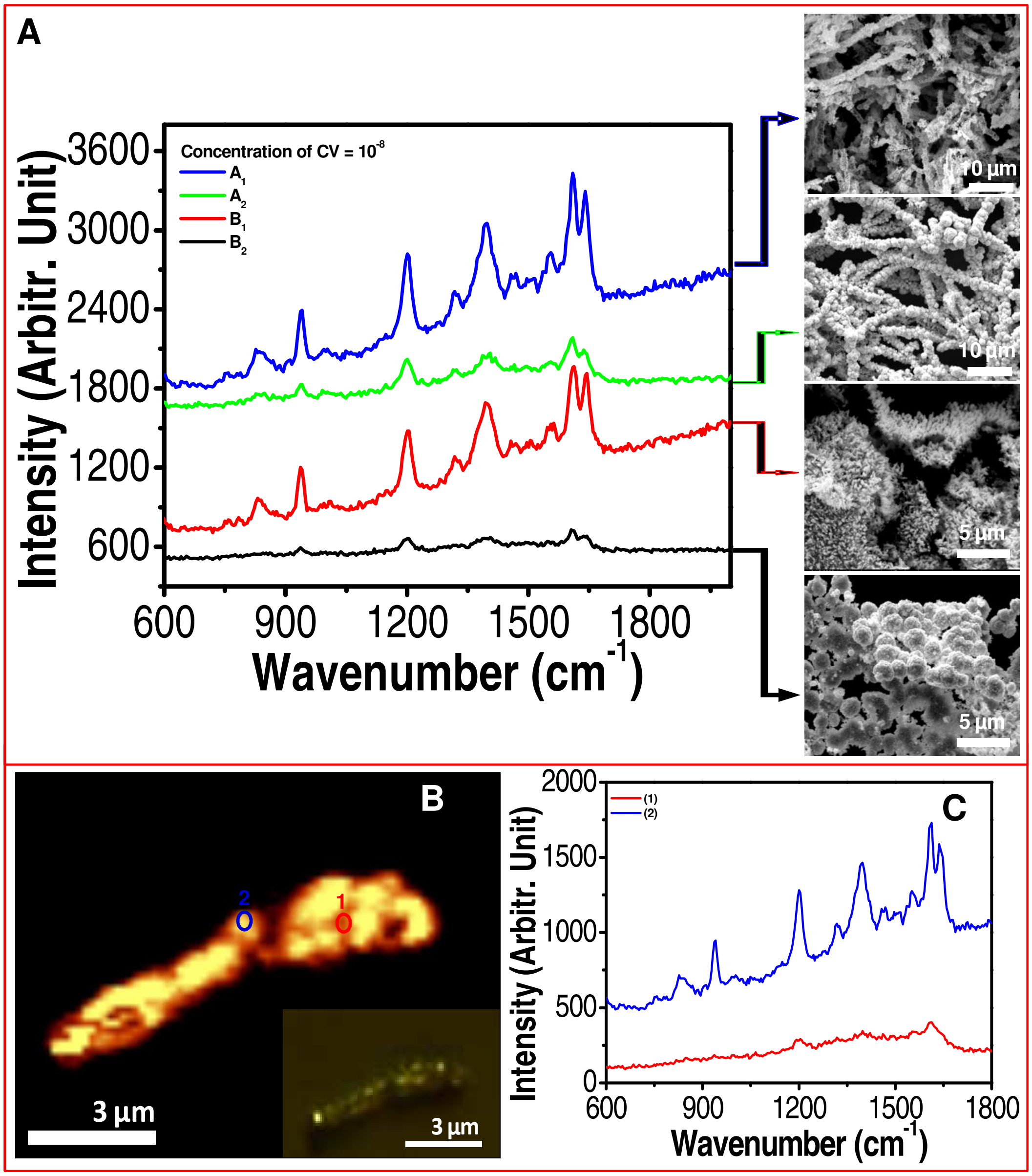

Figure 8. (A) Raman spectra collected from **A1**, **A2**, **B1**, and **B2** upon exposure to 10^{-8} M CV. Representative large area SEM images of each Ni/Au nanosubstrate is shown along with the spectra. (B) Raman image of a Ni/Au nanotube created by integrating the spectral intensities of adsorbed CV between 1200-1700 cm^{-1}. Inset shows the optical image of the nanotube used for Raman imaging. (C) Raman spectra collected the two regions marked in the Raman image shown in B.

The spectra collected from various regions of the nanotube showed varying intensities at different regions (Figure 8C). This can be due to the uneven distribution of gold at the surface of the nanotubes. The more SERS active Au rich region (spot 2) showed higher intensities compared to the Ni rich areas (spot 1) which is not as good as Au in terms of its SERS activity. This result confirms that the deposition of Au onto the Ni NW during the galvanic displacement reaction is not uniform hence there will be slight differences in the intensities of SERS signal at different points.

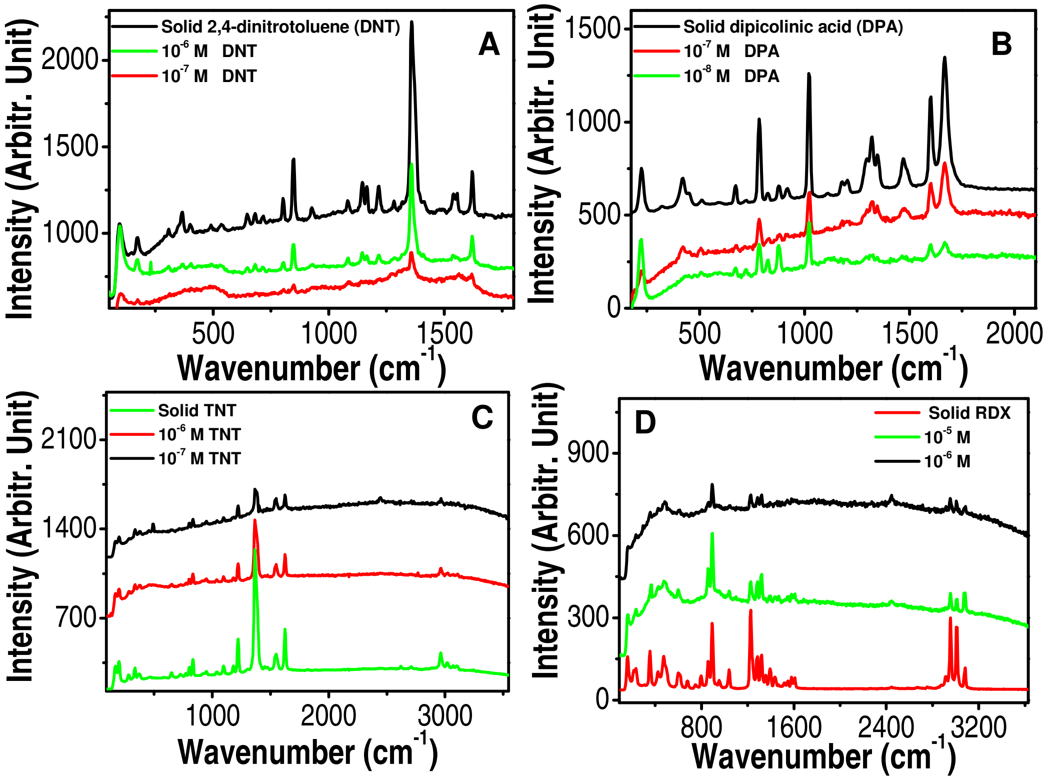

Figure 9. Raman spectra of DNT (A), DPA (B), TNT (C) and RDX (D) solutions of various concentrations adsorbed on $\mathbf{B_1}$. The traces are given in the same intensity scale, but shifted vertically for clarity.

Taking advantages of the high SERS activity of sample **B1**, we demonstrated the utility of this material as an SERS substrate for the detection of certain analytes such as DPA, a molecule which constitutes 5 to 15% of the dry weight of the bacterial spore of *Bacillus anthracis*, the explosives TNT and RDX and an explosive surrogate, DNT. In our study, first we took the Ni/Au NCs on a glass substrate and 20 μL of the analyte solutions of different concentrations were drop-casted. The substrate was subjected to SERS test in ambient air. The back-scattered light was collected using a 60x liquid immersion objective with an integration time of 1s. The enhancement factors (EFs) were calculated in all the cases for a lower detection limit. We could detect the characteristic Raman features of DNT and TNT up to a concentration of 10^{-7} M (EF≈10^{6}) (Figure 9). In the case of DPA, the detection limit was 10^{-8} M (EF≈10^{7}). We could get distinct Raman features up to 10^{-6} M (EF≈10^{5}) for RDX. In all the cases, the resulting Raman features were comparable with the standard solid samples. The multi-analyte detection capability of our SERS substrate makes it highly promising for defense or diagnostics-related applications.

4.3. Reusability of Ni nanocarpet

Further, to demonstrate the reusability of the Ni/Au NCs after each Raman measurement, the substrate was subjected to a sequence of cleaning procedures. Each cycle of cleaning includes washing of the substrate with deionized water (after the SERS measurements) followed by gentle sonication with acetone for about 1 min. The substrate was then kept at 300 ^{0}C for 30 min in a furnace to remove volatile organic components and the resulting substrate was used for further SERS measurements. Even after heat treatment, the surface morphology of the NCs remained almost unchanged. Figure 10A and B show the SEM images of the Ni/Au NCs before and after heat treatment. The resultant substrate was devoid of any Raman features of CV (Electronic supplementary information, Fig. S8†). Even though there is a possibility of oxidation for Ni during heat treatment, it did not affect the SERS activity of the Ni/Au NC as gold is mainly responsible for the SERS enhancement which was quiet stable at that temperature. However, it is to be noted that the adsorption strength of the analyte may also play a role in the reusability of this material. Some molecules may have to be heated well above 300 ^{0}C for complete desorption. So there is a chance of structural tranformation of the NCs which may affect its sensitivity.

After the first cycle of cleaning, the same substrate was used for SERS measurements. The substrate showed similar Raman spectra of CV at a concentration of 10^{-10} M, with its characteristic Raman features with almost the same intensity (Figure 10C). The distance between the substrate and the microscope objective was adjusted so as to get maximum Raman intensity. We checked the reusability of the substrate by measuring the Raman spectra after subsequent washing and cleaning process many times. After each cycle of cleaning, we verified the efficiency of the substrate by collecting the spectra of adsorbed CV. The results obtained using recycled substrates were comparable to the Raman spectra recorded using fresh substrates. The Raman spectra of 10^{-9} M CV collected from the Ni/Au NC after it was subjected for five cycles of cleaning, showed almost all the characteristic features of CV (Electronic supplementary information, Fig. S9†). The SERS sensitivity was found to be decreased upon further use of the same substrate.

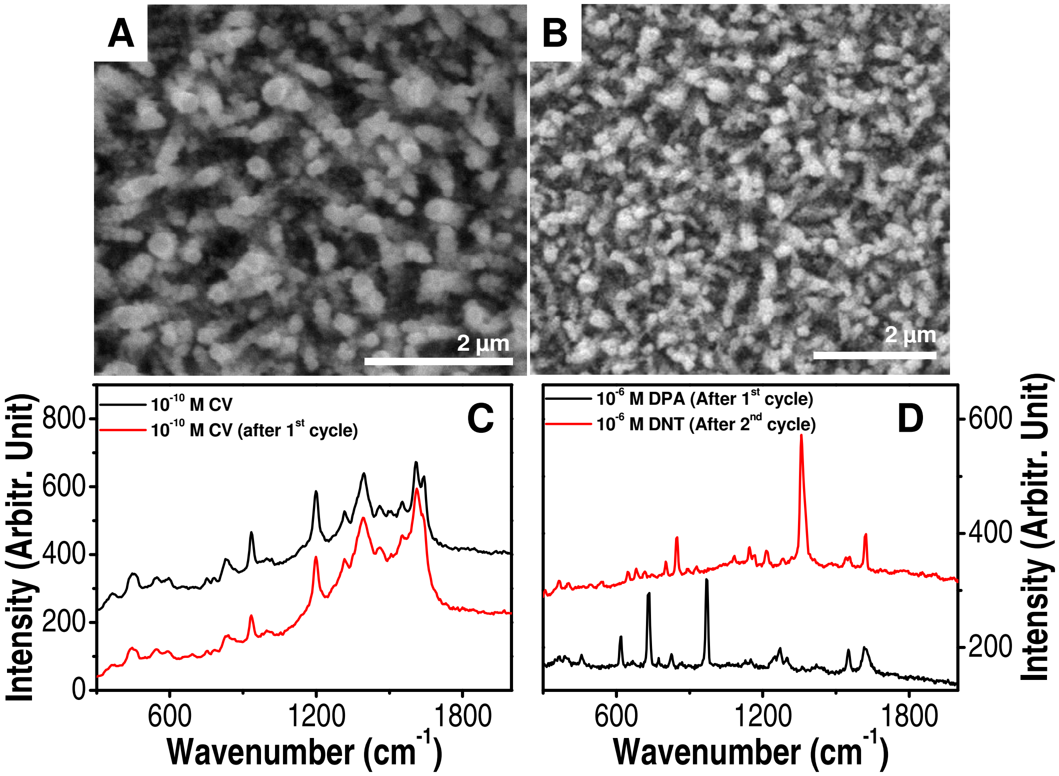

Figure 10. SEM images of the sample $\mathbf{B_1}$ before (A) and after (B) first cycle of cleaning. (C) Raman spectra of 10^{-10} M of CV collected from $\mathbf{B_1}$ before (black trace) and after 1st cycle of cleaning (red trace). (D) Raman spectra of 10^{-6} M of DPA and DNT adsorbed on $\mathbf{B_1}$ after 1st and 2nd cycle of cleaning.

To test the sensitivity of the reprocessed substrates, we conducted the same procedure with different molecules, one after the other on the same substrate. For that, first we used the sample **B$_1$** after the first cycle of cleaning process (previously used for the SERS measurement with CV solution) and drop casted DPA solution of 10^{-6} M concentration. The spectrum collected showed the Raman features of DPA molecule (Figure 10D). The same substrate was subjected to a second cycle of cleaning process and again used for SERS study with a DNT solution of 10^{-6} M. Using that substrate, we could get the distinct Raman features of DNT (Figure 10D).

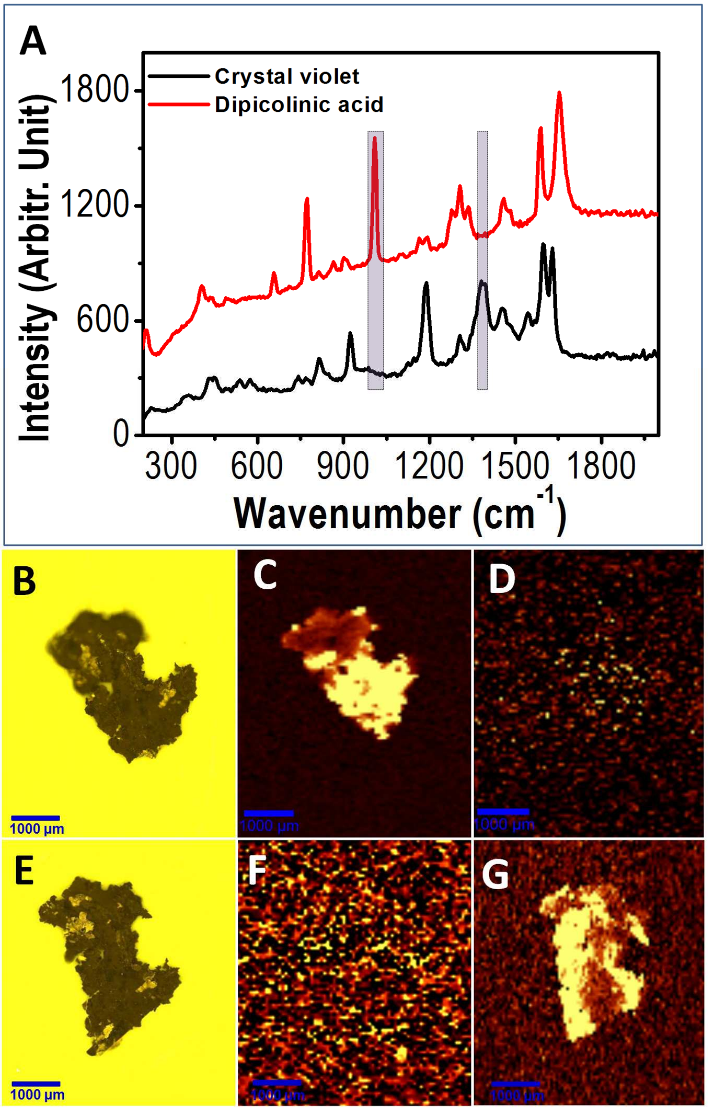

Figure 11. (A) Raman spectrum of 10^{-6} M of CV (black trace) collected from $\mathbf{B_1}$ before 1st cycle of cleaning. Red trace shows the Raman spectrum of 10^{-6} M of DPA adsorbed on the same sample $\mathbf{B_1}$ after 1st cycle of cleaning. B and E are the optical image of $\mathbf{B_1}$ before and after 1st cycle of cleaning, respectively. C and D are the Raman images of $\mathbf{B_1}$ acquired by collecting the Raman intensities of the peaks in the range of 1375-1382 and 1002-1012 cm^{-1}, respectively. 10^{-6} M of CV was used as analyte for the Raman imaging. (D) F and G are the Raman images of $\mathbf{B_1}$ (after first cycle of cleaning) acquired by collecting the Raman intensities of the peaks in the range of 1375-1382 and 1002-1012 cm^{-1}, respectively. Here, DPA (10^{-6} M) was used as analyte for the Raman imaging.

The sensitivity of the recycled Ni/Au NCs towards its SERS activity was further verified by collecting the Raman image of a large area film, before and after recycling, using various analytes such as CV and DPA. We selected two different regions of 1375-1382 and 995-1002 cm^{-1} for imaging due to the reason that CV shows an intense N-phenyl stretching[16] band at 1379 cm^{-1}, which is absent in DPA. At the same time, DPA shows an intense symmetric ring breathing mode[52] at 998 cm^{-1} which is almost absent or weak (appear at 992 cm^{-1} as a weak band) in the case of CV. Figure 11C and D show Raman images of the Ni/Au NC (before recycling) acquired by collecting the Raman intensities of the adsorbed CV in the range of 1375-1382 and 995-1002 cm^{-1}, respectively. The optical image of the Ni/Au NC selected for the Raman imaging is shown in Figure 11B. The Raman image of the Ni/Au NC in C appeared bright and there was no such image in Figure 11D. After the Raman measurements, we carefully cleaned the substrate without any serious damage to the material, treated it with 10^{-6} M of DPA, and collected the Raman image. In this case, we could get the Raman image using intensities in the range of 995-1002 cm^{-1}. But, there was no such image found for the 1375-1382 cm^{-1} range. This indicates that the adsorbed CV molecules were completely removed from the NC after the first cycle of cleaning. The Raman study shows that we can successfully regenerate the NC substrate without losing its sensitivity after recycling.

5. CONCLUSIONS

A facile and cost-effective way to make reusable, highly SERS active, and free-standing large area nanocarpets, extending over cm^2 area, has been developed through a galvanic replacement reaction, starting from prefabricated Ni NCs. Using the same approach we made highly SERS active nanotubes from Ni NWs. We demonstrated the viability of our method to make several hybrid nanoystems such as Ni/Pd nanotubes, Ni/Pt and Ni/Ag NWs in an easy manner by following the same procedure. The high SERS activity of these hybrid materials has been utilized to detect molecules such as dipicolinic acid, dinitrotolune, trinitrotoluene, and RDX at very low concentrations. We verified that the Ni/Au NC can be reused multiple times as SERS substrates without significant loss of its activity. Compared with other conventional SERS substrates, reusable and highly SERS active, large area Ni/Au NCs made by cost-effective way may be a perfect choice for making large area sensors in many practical applications.

Acknowledgements

We thank the Department of Science and Technology, Government of India for constantly supporting our research program on nanomaterials.

†Electronic supplementary information (ESI) available: SEM and EADX data of various materials such as Ni NC and NWs and their hybrid forms, SEM image of branched Ni NWs, XPS spectra of O 1s of various nanomaterials, Raman data showing higher detection limit and reusability of Ni/Au NCs.

REFERENCES

1. M. E. Stewart, C. R. Anderton, L. B. Thompson, J. Maria, S. K. Gray, J. A. Rogers and R. G. Nuzzo, *Chem. Rev.,* 2008, **108**, 494-521.
2. S. R. Nicewarner-Pena, R. G. Freeman, B. D. Reiss, L. He, D. J. Pena, I. D. Walton, R. Cromer, C. D. Keating and M. J. Natan, *Science*, 2001, **294**, 137-141.
3. R. Narayanan and M. A. El-Sayed, *J. Am. Chem. Soc.*, 2004, **126**, 7194-7195.

4. J. P. Xie, Q. B. Zhang, J. Y. Lee and D. I. C. Wang, *ACS Nano*, 2008, **2**, 2473-2480.
5. C. Wang, Y. Chen, T. Wang, Z. Ma and Z. Su, *Adv. Funct. Mater.*, 2008, **18**, 355-361.
6. J. B. Jackson, S. L. Westcott, L. R. Hirsch, J. L. West and N. J. Halas, *Appl. Phys. Lett.*, 2003, **82**, 257-259.
7. M. J. Banholzer, J. E. Millstone, L. Qin and C. A. Mirkin, *Chem. Rev.,* 2008, **37**, 885-897.
8. C. G. Khoury and T. Vo-Dinh, *J. Phys. Chem. C*, 2008, **112**, 18849-18859.
9. P. R. Sajanlal and T. Pradeep, *Nano Res.*, 2009, **2**, 306-320.
10. L. A. Lyon, C. D. Keating, A. P. Fox, B. E. Baker, L. He, S. R. Nicewarner, S. P. Mulvaney and M. J. Natan, *Anal. Chem.*, 1998, **70**, 341R-361R.
11. P. R. Sajanlal and T. Pradeep, *Adv. Mater.*, 2008, **20**, 980-983.
12. J. E. Millstone, S. Park, K. L. Shuford, L. Qin, G. C. Schatz and C. A. Mirkin, *J. Am. Chem. Soc.*, 2005, **127**, 5312-5313.
13. F. Hao, C. L. Nehl, J. H. Hafner and P. Nordlander, *Nano Lett.*, 2007, **7**, 729-732.
14. P. R. Sajanlal and T. Pradeep, *Langmuir*, 2010, **26**, 8901-8907.
15. L. J. Sherry, S.-H. Chang, G. C. Schatz, D. R. P. Van, B. J. Wiley and Y. Xia, *Nano Lett.*, 2005, **5**, 2034-2038.
16. E. S. Shibu, K. Kimura and T. Pradeep, *Chem. Mater.*, 2009, **21**, 3773-3781.
17. E. S. Shibu, J. Cyriac, T. Pradeep and J. Chakrabarti, *Nanoscale*, 2011, **3**, 1066-1072.
18. P. R. Sajanlal, C.Subramaniam, P. Sasanpour, B. Rashidian, and T. Pradeep, *J. Mater. Chem.*, 2010, **20**, 2108.
19. D. P. Fromm, A. Sundaramurthy, P. J. Schuck, G. Kino and W. E. Moerner, *Nano Lett.*, 2004, **4**, 957-961.
20. L. Chen, X. Han, J. Yang, J. Zhou, W. Song, B. Zhao, W. Xu and Y. Ozaki, *J. Colloid Interface Sci.*, **360**, 482-487.

21. O. Peron, E. Rinnert, T. Toury, M. Lamy de la Chapelle and C. Compere, *Analyst*, 2011, **136**, 1018-1022.
22. J. A. Dieringer, A. D. McFarland, N. C. Shah, D. A. Stuart, A. V. Whitney, C. R. Yonzon, M. A. Young, X. Zhang and D. R. P. Van, *Faraday Discuss.*, 2006, **132**, 9-26.
23. L. Au, X. Lu and Y. Xia, *Adv. Mater.*, 2008, **20**, 2517-2522.
24. X. Lu, H.-Y. Tuan, J. Chen, Z.-Y. Li, B. A. Korgel and Y. Xia, *J. Am. Chem. Soc.*, 2007, **129**, 1733-1742.
25. L. Au, Y. Chen, F. Zhou, P. H. C. Camargo, B. Lim, Z.-Y. Li, D. S. Ginger and Y. Xia, *Nano Res.*, 2008, **1**, 441-449.
26. S. E. Skrabalak, J. Chen, Y. Sun, X. Lu, L. Au, C. M. Cobley and Y. Xia, *Acc. Chem. Res.*, 2008, **41**, 1587-1595.
27. A. J. Chung, Y. S. Huh and D. Erickson, *Nanoscale*, 2011, **3**, 2903-2908.
28. Y. Lai, W. Pan, D. Zhang and J. Zhan, *Nanoscale*, 2011, **3**, 2134-2137.
29. V. V. Hardikar and E. Matijevic, *J. Colloid Interface Sci.*, 2000, **221**, 133-136.
30. T. Bala, S. D. Bhame, P. A. Joy, B. L. V. Prasad and M. Sastry, *J. Mater. Chem.*, 2004, **14**, 2941-2945.
31. T. Bala, S. K. Arumugam, R. Pasricha, B. L. V. Prasad and M. Sastry, *J. Mater. Chem.*, 2004, **14**, 1057-1061.
32. P. R. Sajanlal and T. Pradeep, *J. Nanosci. Nanotechnol.*, 2009, **9**, 5283-5287.
33. M. Zhang, J. Deng, M. Zhang and W. Li, *Chin. J. Catal.*, 2009, **30**, 447-452.
34. D.-P. Wang, D.-B. Sun, H.-Y. Yu and H.-M. Meng, *J. Cryst. Growth*, 2008, **310**, 1195-1201.
35. X. Ni, J. Zhang, Y. Zhang and H. Zheng, *J. Colloid Interface Sci.*, 2007, **307**, 554-558.

36. G. Zhang, T. Zhang, X. Lu, W. Wang, J. Qu and X. Li, *J. Phys. Chem. C*, 2007, **111**, 12663-12668.

37. D. Liu, S. Ren, H. Wu, Q. Zhang and L. Wen, *J. Mater. Sci.*, 2008, **43**, 1974-1978.

38. S. Sarkar, A. K. Sinha, M. Pradhan, M. Basu, Y. Negishi and T. Pal, *J. Phys. Chem. C*, **115**, 1659-1673.

39. Y. Wang, Q. Zhu and H. Zhang, *Mater. Res. Bull.*, 2007, **42**, 1450-1456.

40. L. Bai, F. Yuan and Q. Tang, *Mater. Lett.s*, 2008, **62**, 2267-2270.

41. T. S. Sreeprasad, A. K. Samal and T. Pradeep, *Langmuir*, 2007, **23**, 9463-9471.

42. Y. Sun, *Nanoscale*, 2010, **2**, 1626-1642.

43. H. J. Fan, U. Gösele and M. Zacharias, *Small*, 2007, **3**, 1660-1671.

44. A. F. Carley, S. D. Jackson, J. N. O'Shea and M. W. Roberts, *Phys. Chem. Chem. Phys.*, 2001, **3**, 274-281.

45. P. F. Luo, T. Kuwana, D. K. Paul and P. M. A. Sherwood, *Anal. Chem.*, 1996, **68**, 3330-3337.

46. S. K. Sharma, V. Zaporojtchenko, J. Zekonyte, A. Buettner, S. Deki and F. Faupel, *J. Mater. Sci.*, 2004, **39**, 6291-6297.

47. E. N. Esenturk and W. A. R. Hight, *J. Raman Spectrosc.*, 2009, **40**, 86-91.

48. L. Rodriguez-Lorenzo, R. A. Alvarez-Puebla, I. Pastoriza-Santos, S. Mazzucco, O. Stephan, M. Kociak, L. M. Liz-Marzan and d. A. F. J. Garcia, *J. Am. Chem. Soc.*, 2009, **131**, 4616-4618.

49. (a) G. V. P. Kumar, S. Shruthi, B. Vibha, B. A. A. Reddy, T. K. Kundu and C. Narayana, *J. Phys. Chem. C*, 2007, **111**, 4388-4392. (b) E. C. Le Ru, E. Blackie, M. Meyer, P. G. Etchegoin, *J. Phys. Chem. C* 2007**, 111**, 13794-13803. (c) G. Upender, R. Satyavathi, B. Raju, K. Shadak Alee, D. Narayana Rao, C. Bansal, *Chem. Phys. Lett.*2011**, 511**, 309-314.

50. K. Kim, H. J. Jang and K. S. Shin, *Analyst*, 2009, **134**, 308-313.

51. W. Wei, S. Li, J. E. Millstone, M. J. Banholzer, X. Chen, X. Xu, G. C. Schatz and C. A. Mirkin, *Angew. Chem. Int. Ed.*, 2009, **48**, 4210-4212.

52. A. A. Kolomenskii and H. A. Schuessler, *Spectrochim. Acta, Part A: Molecular and Biomolecular Spectroscopy*, 2005, **61**, 647-651.

The table of contents entry

A facile and cost-effective method has been used to make hybrid Ni nanostructures through galvanic replacement reaction from prefabricated Ni nanomaterials and their utility and reusability in the detection of biomolecules, explosives and explosive surrogates at very low concentrations has been demonstrated using Raman spectroscopy and microscopy.

Keyword: functional nanomaterials; SERS; reusable substrate; galvanic replacement reaction; explosives

P. R. Sajanlal and T. Pradeep*